J Arid Land (2025) 17(7): 888–911
doi: 10.1007/s40333-025-0083-x; CSTR: 32276.14.JAL.0250083x

Science Press Springer-Verlag

Quantitative analysis of factors driving the variations in snow cover fraction in the Qilian Mountains, China

JIN Zizhen[1,2], QIN Xiang[3,4*], LI Xiaoying[5], ZHAO Qiudong[4,6], ZHANG Jingtian[7], MA Xinxin[1], WANG Chunlin[1], HE Rui[6], WANG Renjun[3,4]

[1] Department of Geography, Xinzhou Normal University, Xinzhou 034000, China;
[2] Key Laboratory of Ecological Safety and Sustainable Development in Arid Lands, Northwest Institute of Eco-Environment and Resources, Chinese Academy of Sciences, Lanzhou 730000, China;
[3] Qilian Shan Station of Glaciology and Ecological Environment, State Key Laboratory of Cryospheric Sciences, Northwest Institute of Eco-Environment and Resources, Chinese Academy of Sciences, Lanzhou 730000, China;
[4] State Key Laboratory of Cryospheric Sciences, Northwest Institute of Eco-Environment and Resources, Chinese Academy of Sciences, Lanzhou 730000, China;
[5] Department of Computer Science, Xinzhou Normal University, Xinzhou 034000, China;
[6] Key Laboratory of Ecohydrology of Inland River Basin, Northwest Institute of Eco-Environment and Resources, Chinese Academy of Sciences, Lanzhou 730000, China;
[7] State Key Laboratory of Tibetan Plateau Earth System Science (LATPES), Institute of Tibetan Plateau Research, Chinese Academy of Sciences, Beijing 100101, China

Abstract: Understanding the impact of meteorological and topographical factors on snow cover fraction (SCF) is crucial for water resource management in the Qilian Mountains (QLM), China. However, there is still a lack of adequate quantitative analysis of the impact of these factors. This study investigated the spatiotemporal characteristics and trends of SCF in the QLM based on the cloud-removed Moderate Resolution Imaging Spectroradiometer (MODIS) SCF dataset during 2000–2021 and conducted a quantitative analysis of the drivers using a histogram-based gradient boosting regression tree (HGBRT) model. The results indicated that the monthly distribution of SCF exhibited a bimodal pattern. The SCF showed a pattern of higher values in the western regions and lower values in the eastern regions. Overall, the SCF showed a decreasing trend during 2000–2021. The decrease in SCF occurred at higher elevations, while an increase was observed at lower elevations. At the annual scale, the SCF showed a downward trend in the western regions affected by westerly (52.84% of the QLM). However, the opposite trend was observed in the eastern regions affected by monsoon (45.73% of the QLM). The SCF displayed broadly similar spatial patterns in autumn and winter, with a significant decrease in the western regions and a slight increase in the central and eastern regions. The effect of spring SCF on spring surface runoff was more pronounced than that of winter SCF. Furthermore, compared with meteorological factors, a variation of 46.53% in spring surface runoff can be attributed to changes in spring SCF. At the annual scale, temperature and relative humidity were the most important drivers of SCF change. An increase in temperature exceeding 0.04°C/a was observed to result in a decline in SCF, with a maximum decrease of 0.22%/a. An increase in relative humidity of more than 0.02%/a stabilized the rise in SCF (about 0.06%/a). The impacts of slope and aspect were found to be minimal. At the seasonal scale, the primary factors impacting SCF change varied. In spring, precipitation and wind speed emerged as the primary drivers. In autumn, precipitation and temperature were identified as the primary drivers. In winter, relative humidity and precipitation were the most important drivers. In contrast to the other seasons, slope exerted the strongest influence on SCF change in summer. This study facilitates a detailed quantitative description of SCF change in the QLM, enhancing the effectiveness of watershed water resource management and ecological conservation efforts in this region.

*Corresponding author: QIN Xiang (E-mail: qinxiang@lzb.ac.cn)
Received 2024-11-23; revised 2025-05-02; accepted 2025-05-12

Keywords: snow cover fraction; surface runoff; machine learning; histogram-based gradient boosting regression tree (HGBRT) model; hydrological effects; Qinghai-Xizang Plateau

Citation: JIN Zizhen, QIN Xiang, LI Xiaoying, ZHAO Qiudong, ZHANG Jingtian, MA Xinxin, WANG Chunlin, HE Rui, WANG Renjun. 2025. Quantitative analysis of factors driving the variations in snow cover fraction in the Qilian Mountains, China. Journal of Arid Land, 17(7): 888–911. https://doi.org/10.1007/s40333-025-0083-x; https://cstr.cn/32276.14.JAL.0250083x

1 Introduction

Snow is a critical component of the climate system, playing a pivotal role in the global energy and water cycles and serving as an indicator of climate change (Zhang et al., 2019b). Due to its high albedo and ability to store water and heat, snow significantly influences water and energy balance (Frei et al., 2012; Chen et al., 2016). Snowmelt runoff is an important water resource, particularly for alleviating spring drought (Ding and Qin, 2009), and serves as a primary source of river runoff in many mountainous regions (Su et al., 2016). For example, Zhang et al. (2013) concluded that snowmelt runoff contributed approximately 20.36%–30.54% of the total runoff in major basins on the Qinghai-Xizang Plateau, China. In North America, snowmelt runoff accounted for 50.00%–95.00% of the total river runoff (Tuttle et al., 2017). Overall, snowmelt runoff provides water to more than one-six of the global population (Barnett et al., 2005). However, the accumulation and subsequent melting of snow may result in snowstorms, floods, and other disasters (Pomeroy et al., 2016). Therefore, understanding changes in snow cover is crucial for effective water resource management, ecosystem processes, irrigation practice, and disaster mitigation (Xu et al., 2022; Goodarzi et al., 2023).

Global climate change manifested as a pronounced warming trend, particularly over the Qinghai-Xizang Plateau, where temperatures have increased at a rate of 0.17°C/10a over the past 50 a (Chen et al., 2015). Consequently, the extent of snow cover and snow water equivalent have declined across Asian high-elevation regions (Li et al., 2018; Smith and Bookhagen, 2018). Specifically, snow cover dynamics are tightly coupled with climatic variables, and temperature and precipitation are the dominant factors shaping the spatiotemporal variability of snow cover (Notarnicola, 2020). Numerous studies have identified a strong negative correlation between snow cover and temperature; however, the relationship between snow cover and precipitation appears to be more complex and regionally dependent (e.g., Qin et al., 2006; Li et al., 2018). The primary factor impacting snow cover change varies regionally. For example, snow cover decreased slightly by 1.14% between 2001 and 2014 on the Qinghai-Xizang Plateau, primarily under precipitation variability (Li et al., 2018). However, annual snow cover showed an increasing trend in the Altay Mountains, China, with temperature identified as the dominant driver (Qin et al., 2022). Similarly, temperature was found to be a major determinant of snow cover change during 2001–2015 in the Tianshan Mountains (Tang et al., 2017) and on the Loess Plateau (Jin et al., 2015), China. Seasonal sensitivity of snow cover to meteorological drivers also varies: over the Qinghai-Xizang Plateau, snow cover was reportedly more responsive to spring temperature (Wang et al., 2007), while other studies suggested that summer temperature was the main driver (Tahir et al., 2015). Some findings indicated that winter precipitation exerted a great influence on snow accumulation (Wang et al., 2007; Tahir et al., 2015). In the Yarlung Zangbo River Basin, temperature was the predominant factor affecting snow cover fraction (SCF) in spring, summer, and autumn, whereas winter SCF was primarily influenced by precipitation (Guo et al., 2022). In summary, while snow cover change and their drivers have been extensively studied across diverse regions and seasons, regional heterogeneity and seasonal dynamics remain key challenges. Understanding these processes is of critical importance for water resource management and ecological conservation, especially in the arid and semi-arid areas of Northwest China.

Numerous studies have focused only on the impacts of temperature and precipitation on snow cover change (Qin et al., 2006; Li et al., 2018; Qin et al., 2022). However, few studies have considered the impacts of other meteorological factors (such as relative humidity and wind speed) and the combined impacts of meteorological and topographical factors on snow cover change.

Moreover, most existing research lacks a robust quantification of the relative contributions of these drivers to snow cover change. Hence, a quantitative analysis of the impacts of meteorological and topographical factors on snow cover change is of great importance at the watershed or regional scale. Such an analysis will facilitate a detailed quantitative description of factors driving the snow cover change, thereby enhancing the effectiveness of water resource management and ecological conservation efforts in arid and semi-arid areas.

The Qilian Mountains (QLM) are situated in the northeastern part of the Qinghai-Xizang Plateau. It serves as a crucial ecological security barrier in western China and is the source of the three major inland rivers in the Hexi Corridor, China (Li et al., 2015). In recent decades, the region has experienced a marked warming trend (Li et al., 2022; Ren et al., 2024), which is expected to substantially alter snow cover dynamics and regional water availability. Previous studies about the QLM have primarily focused on the spatiotemporal patterns of snow cover and the influence of temperature and precipitation, yet have largely overlooked the roles of additional meteorological and topographical factors, and have rarely quantified their respective contributions (Jiang et al., 2016; Liang et al., 2019). Furthermore, the QLM are characterized by a plateau continental climate shaped by the interplay between westerly circulation and monsoonal systems. The eastern sector is influenced by both the southeast and southwest monsoons, whereas the western sector is predominantly affected by westerlies. Further research is required to identify the extent to which the snow cover change observed in areas jointly influenced by westerly and monsoon winds differs from those in areas where westerly circulation or monsoons are the dominant meteorological processes. In conclusion, an integrated approach that considers meteorological and topographical factors and their respective impacts on snow cover change is essential for accurately quantifying the underlying drivers of variation in snow cover. Such insights are critical not only for managing the Qilian Mountains National Park and supporting the ecological objectives of the Belt and Road Initiative but also for advancing the current understanding of snow cover responses to complex climatic interactions in transitional climate zones.

In this study, we investigated the spatiotemporal variations of SCF in the QLM during 2000–2021 based on a daily cloud-removed SCF dataset constructed from the global surface reflectance product MOD09GA/YD09GA and quantified the impact of topographical (slope and aspect) and meteorological factors (temperature, precipitation, relative humidity, and wind speed) on the variation in SCF in the context of global warming. Finally, we further explored the impact of winter and spring SCF on spring surface runoff. These findings have important implications for watershed water resource management and ecological conservation in the QLM.

2 Materials and methods

2.1 Study area

The QLM (36°–40°N, 94°–104°E; Fig. 1) are located on the northeastern Qinghai-Xizang Plateau. From north to south, the mountain ranges include the Zoulangnan Mountains–Lenglongling Mountains, the Tuolenan Mountains, the Danghenan Mountains, and the Tergun Daba Mountains, etc. It stretches more than 1000 km from east to west and 200–400 km from north to south, with an area of 19.3×10^4 km^2. The terrain gradually rises from southeast to northwest, with an average elevation exceeding 4000 m. The highest peak, Tuanjie Peak, reaches over 5600 m (Xue et al., 2023). The QLM contain extensive cryospheric features, including approximately 2684 glaciers covering a total area 1597.8 (±70.3) km^2 (Guo et al., 2015). Permafrost is also widespread, occupying an area of 8.0×10^4 km^2, which accounts for 47.51% of the total area (Peng et al., 2021). Owing to its inland location and distance from maritime influences, the region experiences a typical continental climate, with a mean annual temperature below 2.00°C. Annual precipitation exhibits a marked altitudinal gradient, increasing from approximately 200.00 mm in the low-mountain zones to around 500.00 mm in higher elevations (Li et al., 2019). As a critical recharge zone for major inland rivers including the Shiyang, Heihe, and Shule rivers of the Hexi Corridor as well as for the upper reaches of the

Yellow River, the QLM play a vital role in sustaining hydrological and ecological stability in western China (Zhang et al., 2014).

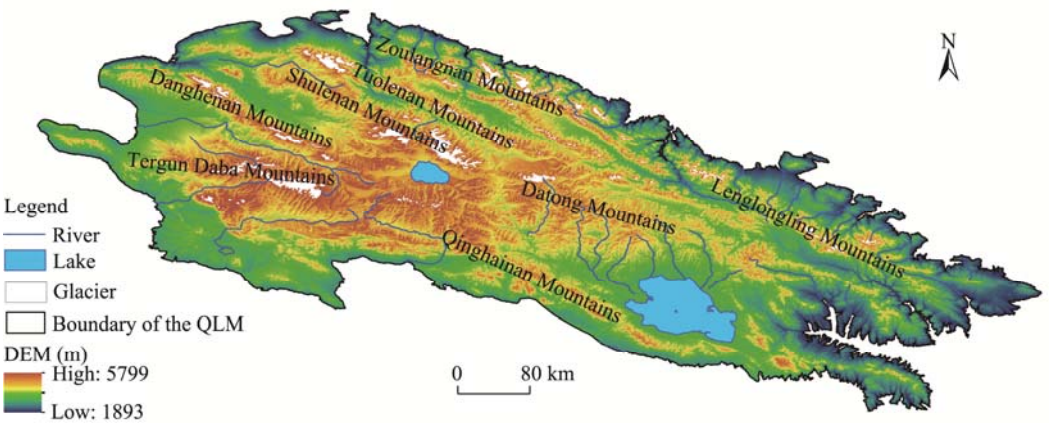

Fig. 1 Overview of the Qilian Mountains (QLM) based on the digital elevation model (DEM)

2.2 Data sources

2.2.1 SCF and runoff data

In this study, SCF data were sourced from the snow cover dataset derived from the Moderate Resolution Imaging Spectroradiometer (MODIS) global surface reflectance product MOD09GA/MYD09GA. It employs a multi-endmember spectral mixture analysis algorithm and a cloud removal algorithm to construct a daily cloud-free snow cover dataset for the Asian Water Tower region from 2000 to 2022, with a resolution of 0.005°. The dataset's accuracy was assessed using 2745 scenes of Landsat-8 imagery, accuracy metrics for SCF—including the coefficient of determination (R^2), root mean squared error (RMSE), and mean absolute error (MAE)—were 0.80, 0.16, and 0.10, respectively (Pan et al., 2024). The data were superior to the commonly used MODSCAG and MOD10A1 snow cover datasets. Therefore, this study employed this dataset to analyze the spatiotemporal variations in SCF and quantitative attribution of SCF change in the QLM. Runoff data were obtained from the European Centre for Medium-Range Weather Forecasts (ECMWF) ReAnalysis 5th Generation-Land (ERA5-Land) (https://cds.climate.copernicus.eu/datasets), offering a spatial resolution of 0.100° and a temporal resolution at the monthly scale and providing an extensive long-term time series spanning from 1950 to the present. The required data for the study area were extracted using the vector boundary of the QLM.

2.2.2 Meteorological and topographical data

The meteorological data employed in this study were obtained from the ERA5-Land dataset, which represents the newest reanalysis datasets produced by the ECMWF. As a state-of-the-art global reanalysis dataset designed for land applications, it is a valuable resource for researchers in this field (Muñoz-Sabater et al., 2021). This reanalysis integrates model data with observational inputs, grounded in the laws of physics. It has a higher resolution than ERA-Interim and ERA5; the spatial resolution is 0.100°×0.100°, and the time series of ERA5-Land spans from 1950 to the present (hourly and monthly datasets). It includes air temperature, total precipitation, relative humidity, wind speed, evaporation, and other climatic elements. Notably, the ERA5-Land temperature product exhibits a strong ability to replicate observed variations across different time scales, making it well-suited for examining temperature trends in the QLM (Zhao and He, 2022). In terms of precipitation, the dataset performs exceptionally well, particularly in the western part of the QLM (Li et al., 2022). For these reasons, ERA5-Land was employed in this study. Additionally, digital elevation model (DEM) data obtained from the Geospatial Data Cloud (https://www.gscloud.cn/) with a spatial resolution of 30 m were used to calculate the slope and aspect of the study area.

2.3 Methods

2.3.1 Sen's trend analysis and Mann-Kendall significance test

This study adopted the method of Sen's trend analysis and the Mann-Kendall significance test to examine the change trend and significance of SCF and various meteorological factors based on the pixel scale. This is a rank-based non-parametric test, which has the advantage of detecting both linear and non-linear trends. The sample is not required to follow a specific distribution and is not affected by outliers, making it particularly suitable for non-normally distributed data in meteorology, hydrology, ecology, and other fields (de Jong et al., 2011). The Sen's trend analysis was conducted by calculating the median of the sequence; however, it does not inherently assess the statistical significance of the trend. The Sen's slope was tested by the Mann-Kendall significance test. The formula for Sen's slope is as follows:

$$\beta = \text{Median}\left(\frac{x_j - x_i}{j - i}\right) \quad (\forall j > i), \tag{1}$$

where β is the Sen's slope; and x_j and x_i are the variable values in the j^{th} and i^{th} year, respectively. When β>0, the time series shows an upward trend, and vice versa.

2.3.2 Quantifying the drivers of SCF change

To quantify the effects of the potential drivers of SCF change across the QLM, we mapped the pixel-wise trends in annual and seasonal SCF in the study area and the pixel-wise trends in climate variables expected to contribute to the SCF change. Then, we fitted a histogram-based gradient boosting regression tree (HGBRT) model that related trends in SCF to topographical factors and trends in climate variables. To focus on pixels with substantial changes in SCF, we restricted this analysis to pixels with SCF trends in the lower/upper (25^{th}/75^{th}) percentile of the 500 m pixels. The selected data were then divided into training and testing sets. The training set was used to train the model and obtain the optimal parameters, while the testing set was used to verify the model's accuracy. We selected the HGBRT approach because regression trees offer a transparent and interpretable means of assessing variable importance, while ensemble techniques like boosting typically enhance model performance by mitigating bias and variance more effectively than single-tree methods (Elith et al., 2008). We fitted the HGBRT using the Python 3.10-based Scikit-learn library, optimizing model hyperparameters through grid search combined with tenfold cross-validation to ensure robust performance (Kohavi, 1995; Pedregosa et al., 2011). The selection of hyperparameters was critical to the performance of machine learning models. Appropriate hyperparameters can greatly improve the model's generalization ability, while poorly chosen ones may result in overfitting or underfitting.

We employed two methods to evaluate the relative importance of each explanatory variable: permutation importance and Shapley values. Permutation importance involved randomly shuffling the values of each explanatory variable across all pixels multiple times and reporting the resulting decrease in the average R^2 value. Shapley values quantified the contribution of each explanatory variable to the predicted value of the response variable. It assigned a "contribution value" to each explanatory variable, reflecting the importance of each variable across different possible combinations. Thus, both metrics aimed to quantify a variable's contribution to explaining the variation in the response, albeit through different methods. We compared both metrics to assess whether our conclusions about the importance of different explanatory variables were robust. Specifically, we calculated permutation importance with 100 permutations using the Scikit-learn implementation and computed Shapley values using the SHAP library (Lundberg et al., 2020). To standardize the two measures of variable importance, we calculated the relative importance of each variable by dividing its importance value by that of the most important variable.

2.3.3 Principal component analysis (PCA)

PCA is a widely used dimensionality reduction technique that transforms high-dimensional data into a lower-dimensional representation while preserving as much of the original information as

possible (Greenacre et al., 2022). It achieves this by constructing a new set of uncorrelated variables—known as principal components—that are linear combinations of the original variables and sequentially capture the maximum possible variance in the data (Jolliffe and Cadima, 2016). In this study, PCA was applied to quantify the contribution of winter and spring temperature, precipitation, wind speed, and SCF to the change in spring surface runoff, thereby identifying the dominant factors driving spring surface runoff variability.

3 Results

3.1 Assessment of model accuracy

Hyperparameter optimization is an indispensable aspect of machine learning practice. The hyperparameters of HGBRT at the seasonal and annual scales are shown in Table 1. Furthermore, Table 2 presents the performance of HGBRT in the QLM at the seasonal and annual scales. The R^2 values in spring, summer, autumn, and winter, and at the annual scale were greater than 0.77. Additionally, the RMSEs of the testing set were less than 0.20%. These values indicated that the HGBRT is highly applicable to the QLM.

Table 1 Hyperparameters of HGBRT at the seasonal and annual scales

Parameter	Spring	Summer	Autumn	Winter	Annual
Learning_rate	0.03	0.01	0.02	0.01	0.02
Max_bin	173	162	202	171	161
Max_iter	1400	1800	1500	1700	1600
Max_depth	50	51	58	43	56

Note: HGBRT, histogram-based gradient boosting regression tree; Max_bin, the maximum number of bins; Max_iter, the maximum number of iterations; Max_depth, the maximum depth of tree.

Table 2 Performance of HGBRT at the seasonal and annual scales

Statistical result	Spring	Summer	Autumn	Winter	Annual
RMSE of the entire dataset (%)	0.11	0.03	0.11	0.10	0.10
R^2 of the entire dataset	0.93	0.75	0.88	0.77	0.85
RMSE of the training set (%)	0.04	0.02	0.04	0.05	0.08
RMSE of the testing set (%)	0.19	0.13	0.20	0.18	0.16

Note: RMSE, root mean squared error; R^2, coefficient of determination.

3.2 Spatiotemporal distributions of SCF

Figure 2a presents the variation in monthly SCF that was averaged over the QLM during 2000–2021. The monthly distribution exhibited a bimodal pattern. Specifically, the mean SCF increased from September to November, decreased in December, and increased in January of the following year. Additionally, the mean SCF decreased from January to August. The peak mean SCF values were 20.82% in January, while the lowest value, approximately 1.51%, occurred in August. The annual mean SCF over the entire QLM was approximately 11.49% during the study period, covering an area of approximately 2.2×10^4 km^2. The mean SCF at different elevation zones increased with elevation: there was a gentle increase and a mean SCF of 7.63% below 4500 m, and a more rapid increase and a mean SCF of 66.64% above 4500 m (Fig. 2b). The maximum SCF, approximately 92.93%, was observed at elevations above 5500 m. This pattern was primarily driven by lower temperatures and higher precipitation at higher elevations, which favor snow accumulation and preservation. Higher temperatures and less precipitation are not conducive to preserving snow at lower elevations. The snow-covered areas were predominantly concentrated at elevations between 3500 and 5000 m, accounting for approximately 80.14% of the total snow-covered area. An additional 15.83% was distributed between 2000 and 3500 m, while only 4.12% of the snow-covered area was found above 5000 m.

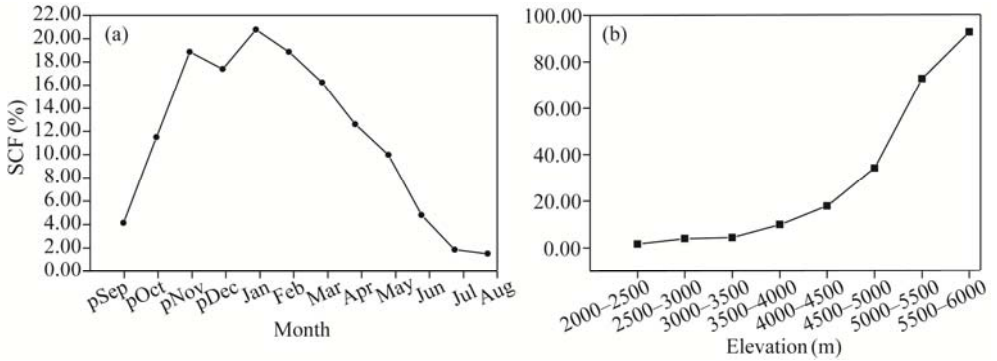

Fig. 2 Variations in monthly snow cover fraction (SCF) from September of the previous year to August (a) and annual SCF at different elevation zones (b) over the QLM during 2000–2021. pSep, pOct, pNov, and pDec represent September, October, November, and December of the previous year, respectively.

Figure 3 shows the monthly SCF changes for different elevation zones over the QLM during 2000–2021. The SCF exhibited a bimodal pattern for all elevation zones at elevations above 3500 m. The lower the elevation, the closer the occurrence of two peaks. At the elevation zone of 5500–6000 m, the SCF reached its peak value (approximately 96.89%) in April, and the secondary peak (approximately 94.64%) occurred in October of the previous year. The lowest SCF (approximately 84.36%) occurred in August due to the stronger sublimations at elevations between 5500 and 6000 m. At the elevation zone of 5000–5500 m, the SCF reached its maximum in March, and the secondary peak occurred in November of the previous year. Compared to the 5500–6000 m elevation zone, the primary SCF peak occurred one month earlier, while the secondary peak was delayed by one month within this elevation zone. The peak occurrence at the elevation zone of 4500–5000 m exhibited temporal synchronicity with peak occurrence at the 5000–5500 m elevation zone. At the 4000–4500 m elevation zone, the SCF reached its maximum in November of the previous year. The secondary peak occurred two months earlier compared to the SCF at the 4500–5000 m elevation zone. The pattern at the elevation zone of 3500–4000 m was consistent with that at the 4000–4500 m elevation zone. In high-elevation regions, lower temperatures led to increased precipitation in spring and autumn, primarily in the form of snowfall. Consequently, the time interval between two peak precipitation periods was relatively long. Conversely, low-elevation regions experienced higher temperatures, with snowfall occurring primarily in winter during a relatively short time interval.

The SCF at the 4500–5000 m elevation zone was markedly lower than that above 5000 m. Below 4500 m, snowpack began accumulating in October of the previous year, peaked in January (approximately 4.74%–30.59%), and decreased to less than 2.00% in July. Generally, the SCF at higher elevations was larger and lasted longer than that at lower elevations throughout the seasons. Additionally, the onset of snowmelt occurred later at the increased elevations. Furthermore, SCF exhibited a notable decline after May at elevations above 4500 m, while a more pronounced reduction was observed after February or March at elevations below 4500 m. Snow accumulation occurred in autumn, winter, and spring months at elevations above 4500 m, whereas below 4500 m, it predominantly occurred between October of the previous year and January.

Figure 4 illustrates the spatial distribution of seasonal and annual multi-year average SCF over the QLM during 2000–2021. At the annual scale, a clear spatial variability of SCF can be observed in the QLM with higher SCF in the west and lower SCF in the east. Moreover, the SCF increased with the rise in elevation. In the eastern part of the QLM, high SCF was primarily concentrated in the Lenglongling Mountains, influenced by the monsoon and higher elevations (with a maximum elevation of 5255 m). In the western part of the QLM, high SCF areas were concentrated in the Tergun Daba Mountains, Danghenan Mountains, and Shulenan Mountains, driven by the westerly circulation and higher elevations. The areas with SCF less than 20.34% covered 82.47% of the total area in the QLM. The snow-free areas were located near the main river valleys (Figs. 1 and 4e).

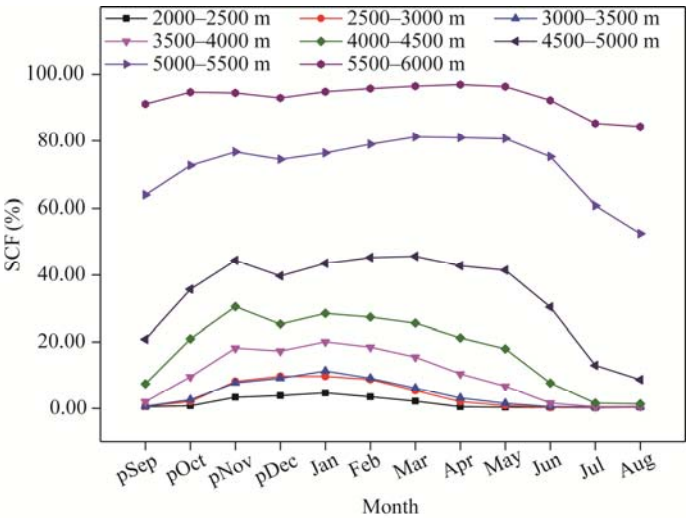

Fig. 3 Variations in monthly SCF at different elevation zones in the QLM from September of the previous year to August during 2000–2021

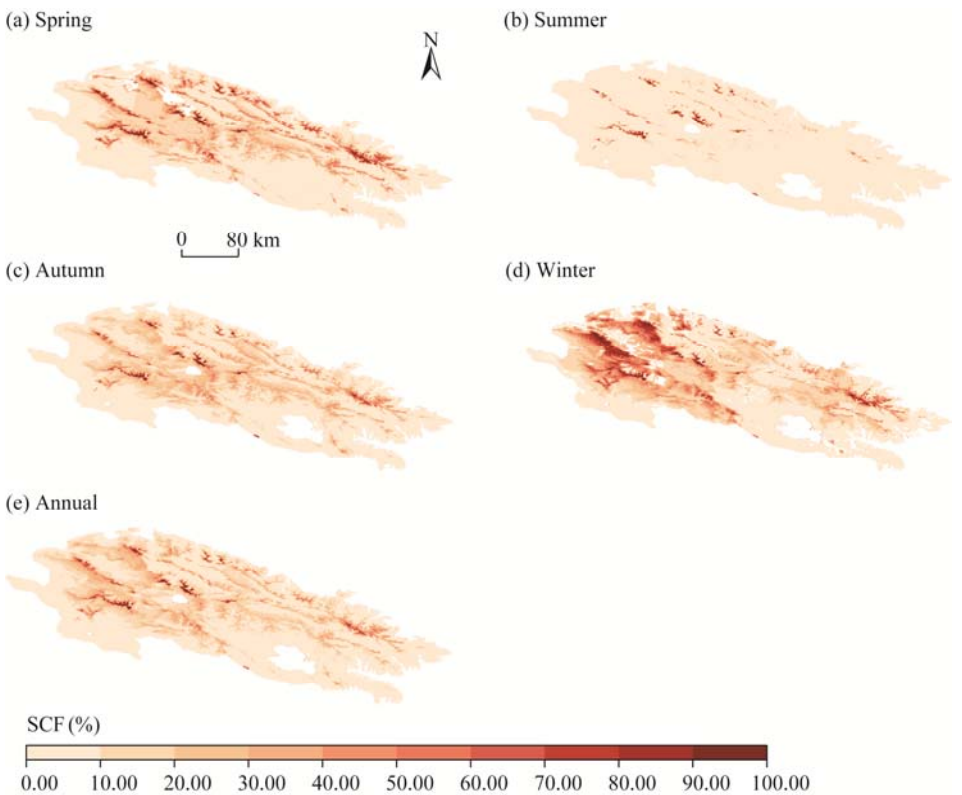

Fig. 4 Spatial distributions of seasonal multi-year average SCF in spring (a), summer (b), autumn (c), and winter (d) as well as annual multi-year average SCF (e) in the QLM during 2000–2021

At the seasonal scale, the SCF reached its lowest point in summer. However, the high values (>80.04%) were maintained at the higher elevations of the western mountains. The SCF gradually increased in autumn, rising from less than 10.00% to 10.00%–20.00% or more in most areas. The areas with SCF of 10.00%–20.00% and more than 50.00% accounted for 20.94% and 1.64% of the QLM, respectively. The SCF reached a maximum in winter, with the area proportion (23.54%) of SCF between 10.00% and 20.00% showing a modest increase compared to autumn, while the

area proportion for SCF>50.00% (8.43%) showed a more pronounced increase. Generally, the increase of SCF was notably faster in the west than in the east. By spring, SCF began to decline as the temperature rose and snow melted, especially in the west, where areas with SCF<50.00% accounted for 4.33% of the QLM.

3.3 Spatiotemporal variations of SCF

Figure 5 illustrates the interannual variation in SCF across different elevation zones and in different seasons. The SCF declined before 2013 and increased afterward, showing an overall non-significant decreasing trend (Fig. 5a). Furthermore, a non-significant increasing trend of SCF was observed in spring and summer at rates of 0.12%/a and 0.01%/a, respectively. Conversely, a decreasing trend was observed in autumn (0.05%/a) and winter (0.09%/a). Notably, the most pronounced decline occurred in winter, serving as the primary contributor to the overall reduction in annual SCF.

Across different elevation zones, SCF exhibited a generally decreasing trend, except for the 3500–4000 and 4000–4500 m elevation zones, where the SCF showed a slight increase and the area accounted for approximately 36.62% of the total area. The reduction rate of SCF increased with elevation, with a substantial decrease (0.26%/a) occurring at elevations above 5000 m.

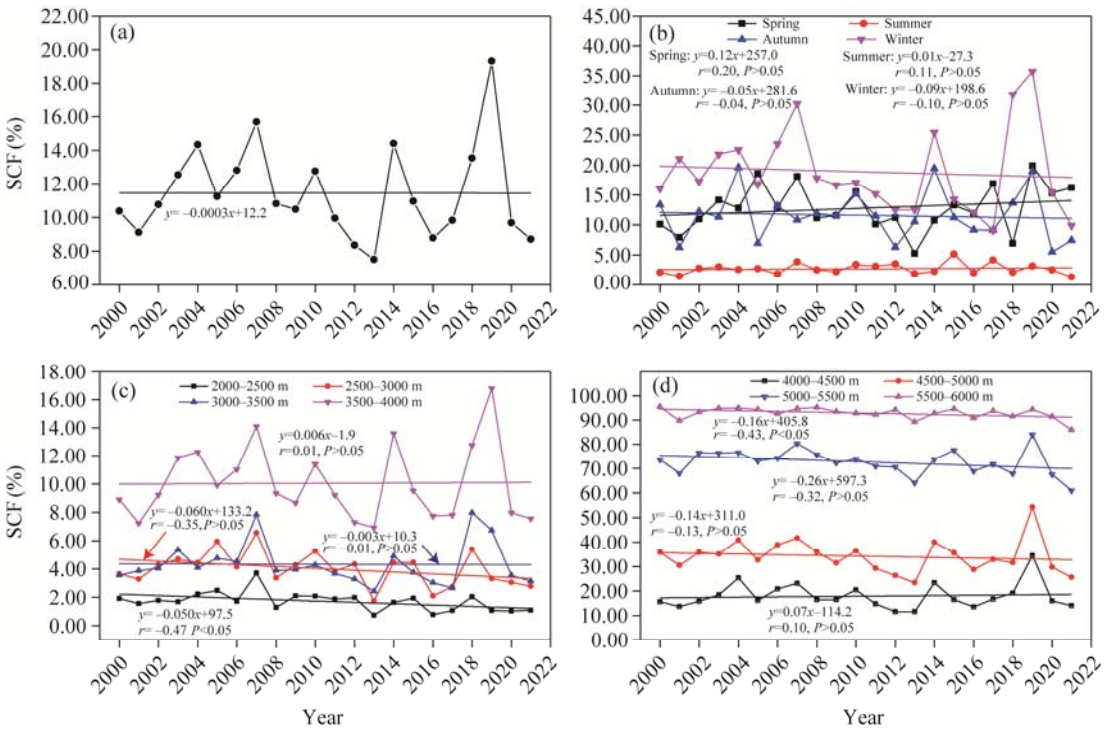

Fig. 5 Interannual variations in SCF at the annual scale (a) and seasonal scale (b), as well as at different elevation zones (c and d) during 2000–2021

The annual and seasonal change trends of SCF also demonstrated marked spatial heterogeneity (Fig. 6a–e). Concerning annual changes, a decline in SCF was observed across most of the western regions and along the northern and eastern margins, accounting for 52.84% of the total area (with 8.59% of regions showing substantial reductions). Conversely, increasing trends were primarily concentrated in the central regions and parts of the eastern regions, accounting for about 45.73% of the total area (with 5.23% of regions showing substantial increases). The decrease in SCF predominantly observed in regions with high SCF at higher elevations. In comparisons, the increases in SCF were mainly evident in areas with relatively low SCF at lower elevations in the eastern and central parts of the mountains. This outcome suggested a distinct elevational disparity in the spatial dynamics of SCF change.

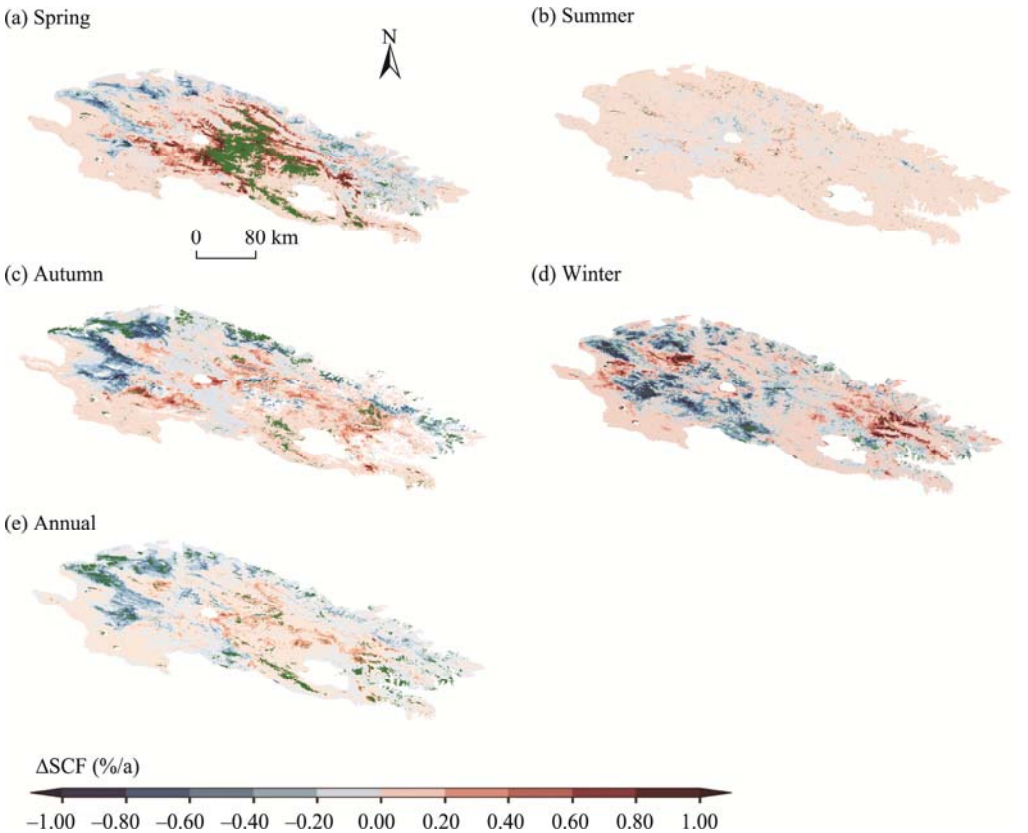

Fig. 6 Spatial distributions of trend in SCF in spring (a), summer (b), autumn (c), and winter (d), as well as at the annual scale (e) during 2000–2021. The green dots indicate the areas showing significant change trend at $P<0.05$ level. Δ denotes the rate of change.

Regarding seasonal changes, an increasing trend in SCF was observed in spring across most areas of the QLM, with the most pronounced increase occurring in the central regions. These regions accounted for approximately 44.89% of the QLM (with regions showing significant increase in SCF making up 20.34% of the QLM). However, a slight decline was observed in a minority of areas in the eastern and western regions, collectively accounting for approximately 30.04% of the QLM (with regions showing significant decrease in SCF only accounting for 3.72% of the QLM). In summer, the SCF exhibited minimal or inconspicuous variations, with a slight increasing tendency observed in the certain regions. Specifically, the regions exhibiting a negative trend in SCF accounted for 12.21% of the QLM, while those with a positive trend comprised 22.59% of the QLM. In autumn, the SCF in most of the western regions and the northern edge exhibited a decreasing trend, accounting for 45.89% of the QLM (with a significant decrease accounting for 7.91% of the QLM). In contrast, most of the central and eastern regions (comprising 34.89% of the QLM) showed an increasing trend in SCF, with a significant increase accounting for 4.91% of the QLM. In winter, most of the western regions and a small portion in the east showed a decreasing trend in SCF. No significant changes were observed in the central regions. The areas exhibiting a decrease in SCF accounted for 57.94% of the QLM (with a significant decrease accounting for 4.29% of the QLM). In contrast, the areas showing an increase in SCF accounted for only 26.54% of the QLM (with a significant increase accounting for 1.33% of the QLM). This outcome indicated a notable reduction in SCF in winter, which was the primary driver of the overall decrease in annual SCF.

In conclusion, the smallest variations in SCF were observed in summer, followed by autumn, while winter and spring exhibited a more significant fluctuation. Regardless of the annual or

seasonal scale, the regions influenced by the monsoon in the east exhibited an increasing trend in SCF. In contrast, the western regions influenced by the westerly circulation displayed a decreasing trend in SCF, particularly in winter.

3.4 Relationship of SCF with meteorological and topographical factors

3.4.1 Interannual variations in temperature and precipitation

Figure 7 shows the spatial distributions of multi-year average temperature and multi-year average precipitation and their interannual variations during 2000–2021. Temperature was higher in the eastern regions and lower in the western regions, exhibiting a decreasing gradient from east to west (Fig. 7a). The multi-year average temperature was –2.74°C in the QLM, with an overall increasing trend at a rate of 0.03°C/a. Similarly, a decreasing trend from east to west was observed in precipitation (Fig. 7b). The multi-year average precipitation was 247.00 mm with an increase rate of 0.48 mm/a. The average annual temperature exhibited an upward trend from 2000 to 2021 (Fig. 7c). Both the eastern and western regions exhibited an increasing trend, while the central region showed relatively minor changes. Additionally, the annual precipitation demonstrated an upward trend, with a more pronounced increase in the southern regions than in their northern counterparts (Fig. 7d). These observations suggested a general shift toward a warmer and more humid climate in the QLM.

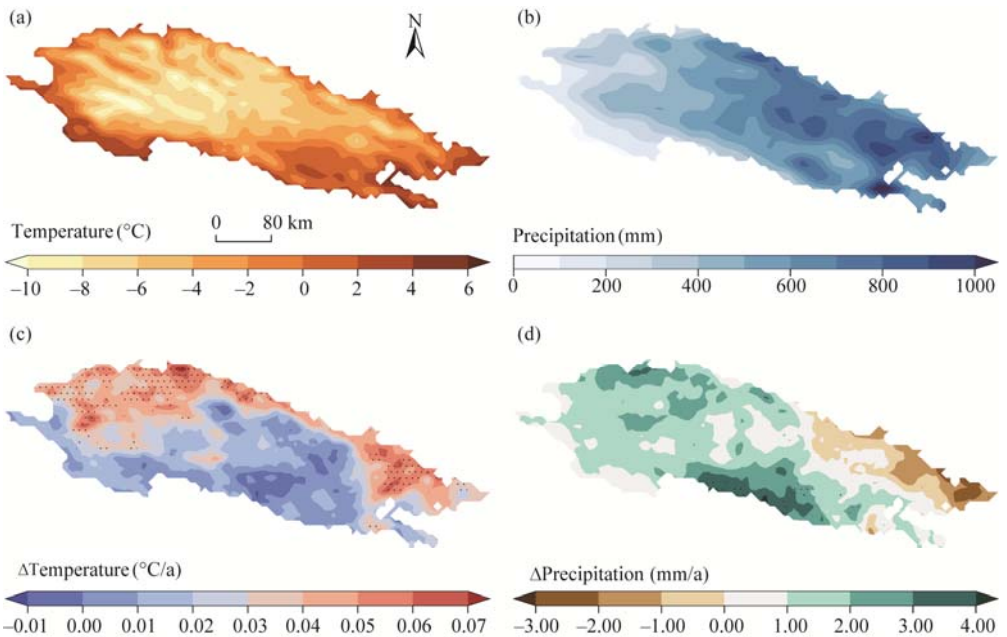

Fig. 7 Spatial distributions of multi-year average temperature (a), multi-year average precipitation (b), interannual variation of average annual temperature (c), and interannual variation of annual precipitation (d) during 2000–2021. The green dots indicate the areas showing significant change trend at $P<0.05$ level.

At the seasonal scale, the increase of temperature was most pronounced in spring, followed by autumn, summer, and winter (Table 3). Notably, the warming rate in spring exceeded that in the other seasons across the QLM. The spring and summer precipitation exhibited an increasing trend, while the autumn and winter precipitation showed an increasing trend. Overall, the increase in summer precipitation contributed to the rise in annual precipitation. Additionally, relative humidity showed an increasing trend in spring and summer and a decreasing trend in other seasons. In contrast, wind speed showed a decreasing trend in all seasons.

Table 3 Trends of meteorological factors at the seasonal and annual scales

	Spring	Summer	Autumn	Winter	Annual
Temperature (°C/a)	0.05	0.01	0.03	0.00	0.03
Precipitation (mm/a)	0.18	0.80	–0.38	–0.11	0.48
Relative humidity (%/a)	0.06	0.18	–0.04	–0.15	0.01
Wind speed (m/(s•a))	–0.011	–0.001	–0.005	–0.001	–0.004

3.4.2 Quantitative analysis of factors driving the SCF change

This study quantified the effects of meteorological factors, including precipitation, temperature, relative humidity, and wind speed, as well as topographical factors, such as slope and aspect, on SCF at annual and seasonal scales using the HGBRT (Fig. 8). At the annual scale, the results revealed that temperature and relative humidity were the most influential factors driving the SCF change. Notably, temperature showed a negative correlation with SCF, while relative humidity was positively correlated with SCF. Relative humidity increased obviously in summer, at a rate of 0.18%/a, whereas SCF was minimal and showed the least variation in summer. Thus, compared to the temperature, relative humidity exerted a comparatively minor influence on SCF, and the impact of precipitation on SCF was similarly negligible. We explored the influence of individual factors on SCF change (Fig. 9). When the rate of temperature increase exceeded 0.04°C/a, SCF exhibited a pronounced decline, reaching a maximum reduction of approximately 0.22%/a. Conversely, when the temperature rise remained below 0.04°C/a, SCF tended to remain relatively stable. Regarding relative humidity, an increase rate exceeding 0.02%/a corresponded to a stabilized SCF rise of approximately 0.06%/a, suggesting a threshold effect in the response of SCF to changes in atmospheric moisture. Temperature increased at a higher rate than relative humidity (Table 3). It can be concluded that rising temperatures primarily drove the modest decline in annual SCF. Concerning topographical factors, slope and aspect had a smaller impact on annual SCF compared to the impact from meteorological factors.

In spring, precipitation and wind speed emerged as the primary drivers of SCF variability (Fig. 8a). Precipitation exhibited an increasing trend over the study period, while wind speed generally declined (Table 3). SCF increased concurrently with rising precipitation and decreasing wind speed (Fig. 10a and b), suggesting that these two factors jointly contributed to the observed enhancement of SCF in spring. Specifically, when the increase in precipitation was less than 0.50 mm/a, SCF exhibited limited variation and generally declined. In contrast, when the precipitation increase exceeded 0.50 mm/a, SCF responded with a marked upward trend, reaching a maximum value of approximately 0.31%/a. The frequency distribution of precipitation increases exceeding 0.50 mm/a exhibited a relatively concentrated distribution (Fig. 10a). An increase in SCF was observed when the wind speed decreased by more than 0.015 m/(s•a). Conversely, when the reduction in wind speed was less than 0.010 m/(s•a), SCF exhibited a notable decline (the frequency within this range was relatively low) (Fig. 10b). Furthermore, SCF showed a decreasing trend when the temperature increased at a rate exceeding 0.06°C/a (the frequency of temperature increases greater than 0.06°C/a was relatively low) (Fig. 10c). Regarding topographical factors, slope and aspect exerted the least influence on spring SCF (Fig. 10d and e). In conclusion, the area exhibiting an increase in SCF was relatively extensive in spring, encompassing approximately 45.00% of the total area.

In contrast to the other seasons, slope exerted the strongest influence on SCF change in summer (Fig. 8b). Snow was primarily distributed in high-elevation regions, where slope generally increased with elevation, especially in areas with slopes below 25° (Fig. 11). The effects of temperature and wind speed on SCF were secondary (Fig. 12). Although temperature exhibited an increasing trend, its impact on SCF remained minimal. Additionally, a decrease in wind speed was observed across most regions within the QLM, resulting in a slight increase in SCF. Relative humidity and precipitation also exerted relatively weak effects on SCF. Consequently, the changes in SCF were relatively inconspicuous in summer.

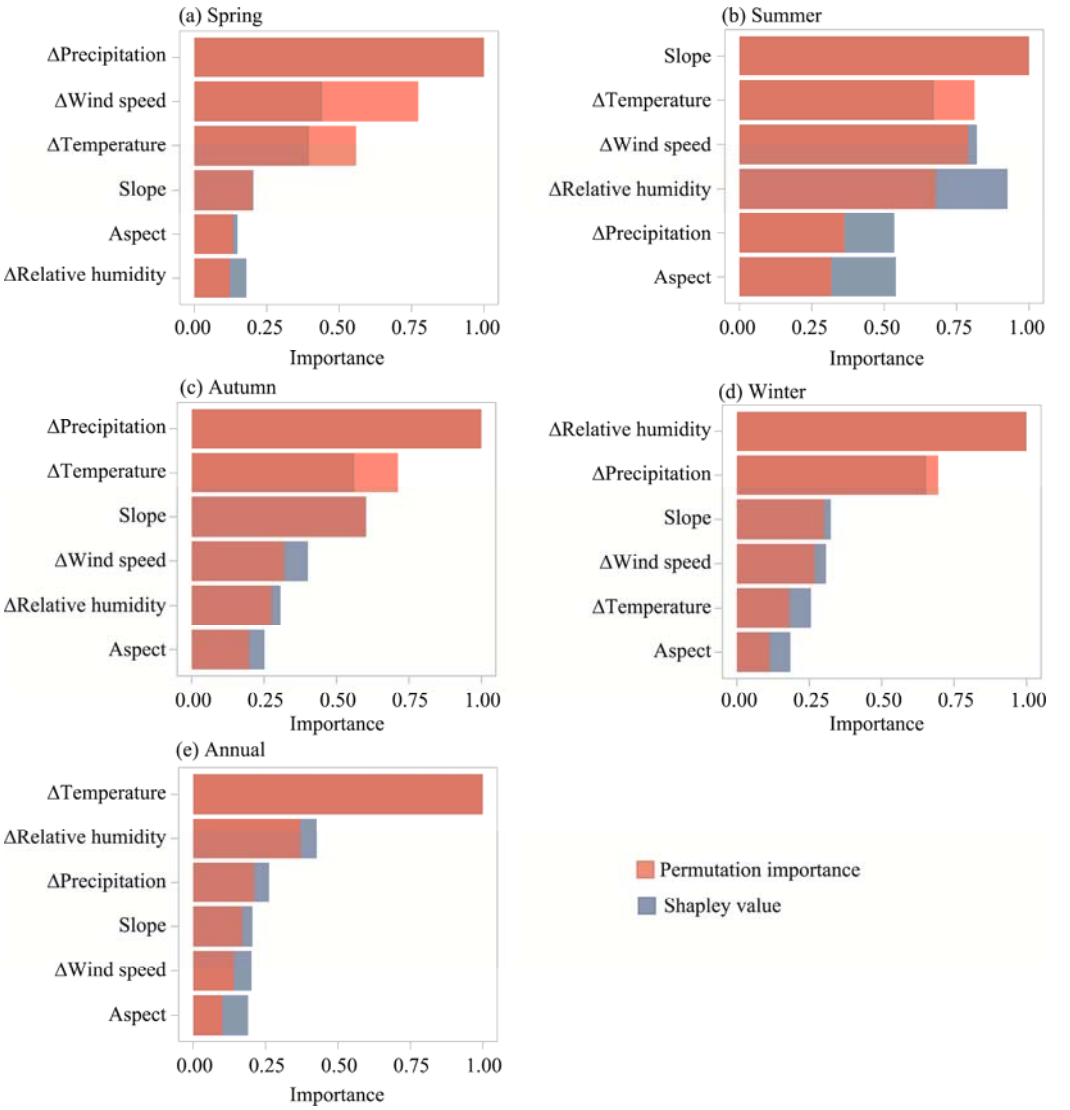

Fig. 8 Ranking of the impacts of various factors on SCF in spring (a), summer (b), autumn (c), and winter (d), as well as at the annual scale (e)

In autumn, precipitation and temperature were identified as the primary drivers of SCF variations (Fig. 8c). Precipitation decreased while temperature increased in the QLM (Table 3). SCF showed a positive correlation with precipitation and a negative correlation with temperature (Fig. 13). Specifically, in most regions, precipitation rapidly decreased during autumn (precipitation encompasses snowfall and rainfall events). A reduction in precipitation greater than 1.00 mm/a was associated with a maximum decline in SCF (0.15%/a). Furthermore, when temperature increased by less than 0.04°C/a, the vatiations in SCF were insignificant. However, when temperature exceeded 0.04°C/a (the temperature increased by more than 0.04°C/a in some regions), a notable decline in SCF occurred, with a maximum reduction of approximately 0.08%/a. Consequently, a reduction in SCF was observed in certain regions (45.95% of the total area). Furthermore, a decline in wind speed was observed in some regions, with a decrease of less than 0.005 m/(s·a) leading to a significant increase in SCF. The increase in SCF in certain regions (34.94% of the total area) was primarily attributed to the reduction in wind speed. Relative humidity and aspect exerted the least impact on SCF change.

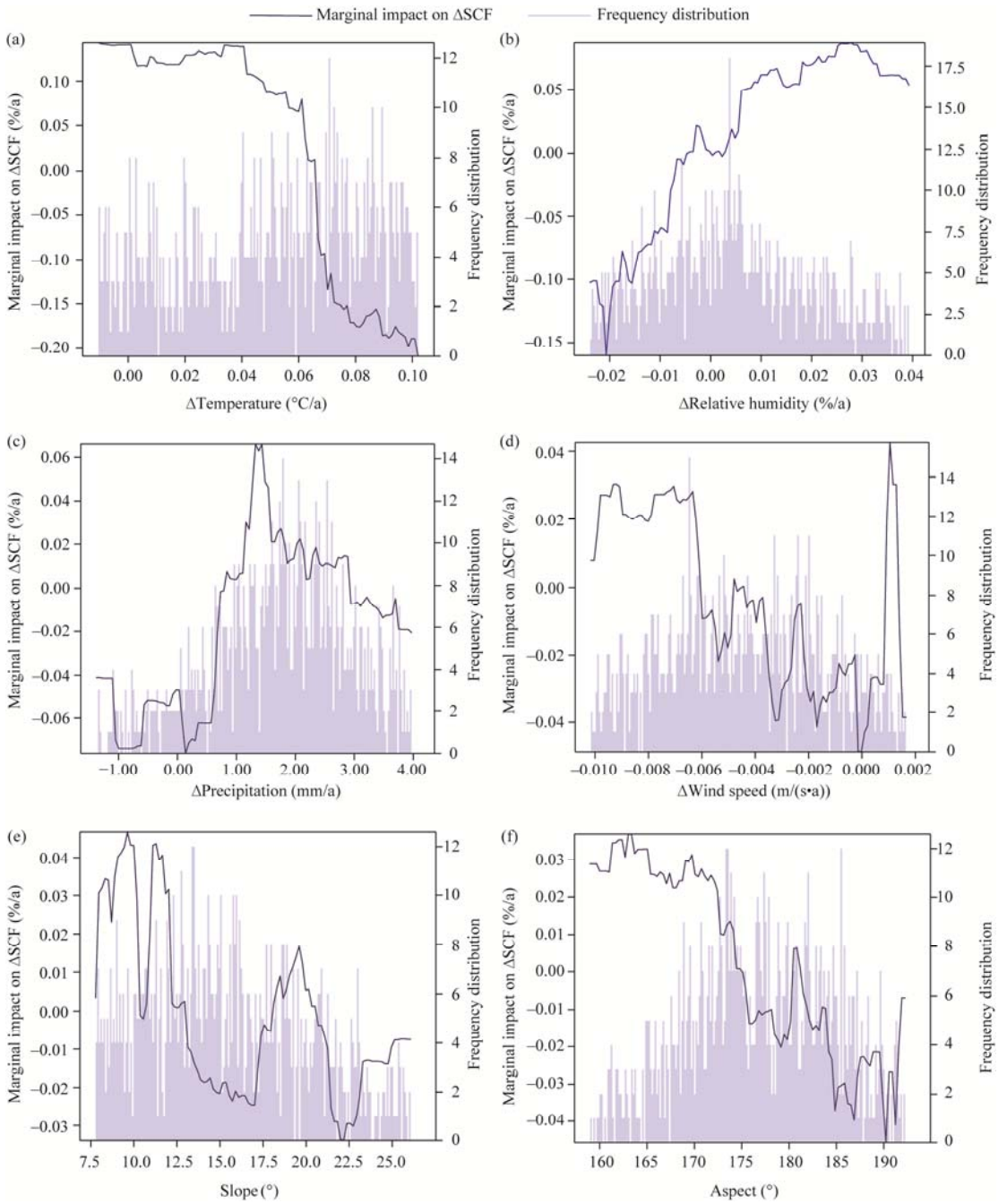

Fig. 9 Partial dependence plots for the impacts of temperature (a), relative humidity (b), precipitation (c), wind speed (d), slope (e), and aspect (f) on SCF change at the annual scale

In winter, relative humidity and precipitation were the primary drivers of SCF change, both exhibiting a positive correlation with SCF (Figs. 8 and 14). Relative humidity and precipitation displayed a declining trend in the QLM (Table 3). Additionally, the maximum reduction in SCF was approximately 0.15%/a for relative humidity and 0.33%/a for precipitation (Fig. 14). Compared to autumn, precipitation in winter had a greater impact on SCF due to its occurrence in the form of snowfall. Furthermore, an increase in temperature led to a decrease in SCF. Consequently, SCF decreased in most regions (57.89% of the total area). Besides, the impact of wind speed on SCF in winter differed from its impact in other seasons, being positively

correlated. Wind speed increased in approximately half of the regions, leading to increased SCF in some areas (26.54% of the total area). Aspect had the least impact on SCF in winter.

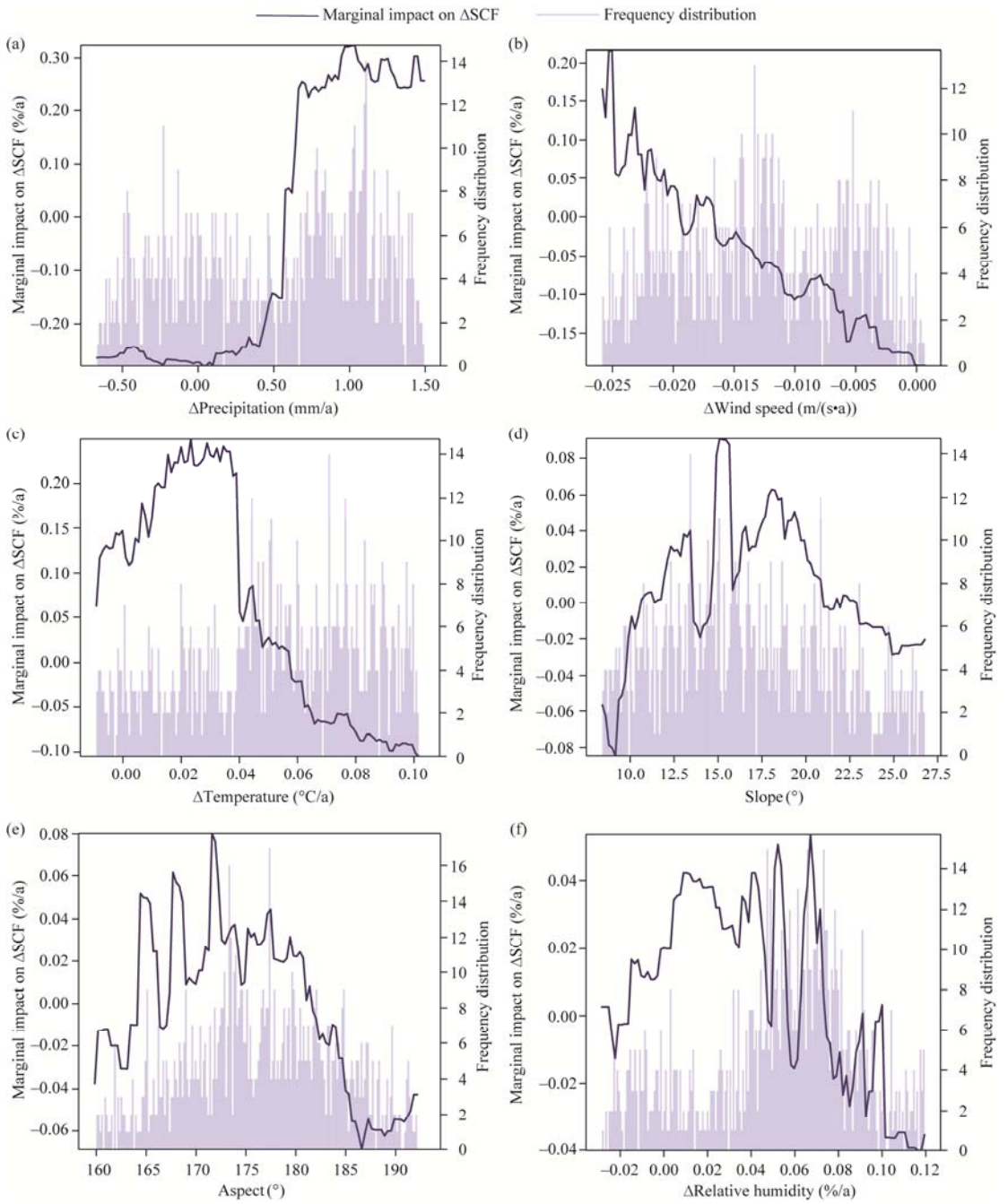

Fig. 10 Partial dependence plots for the impacts of precipitation (a), wind speed (b), temperature (c), slope (d), aspect (e), and relative humidity (f) on SCF change in spring

4 Discussion

4.1 Spatiotemporal dynamics of SCF and its driving factors

A significant spatial variation in SCF was observed across different climatic zones. In monsoon-dominated basins, the highest SCF occurred between October and February, reaching

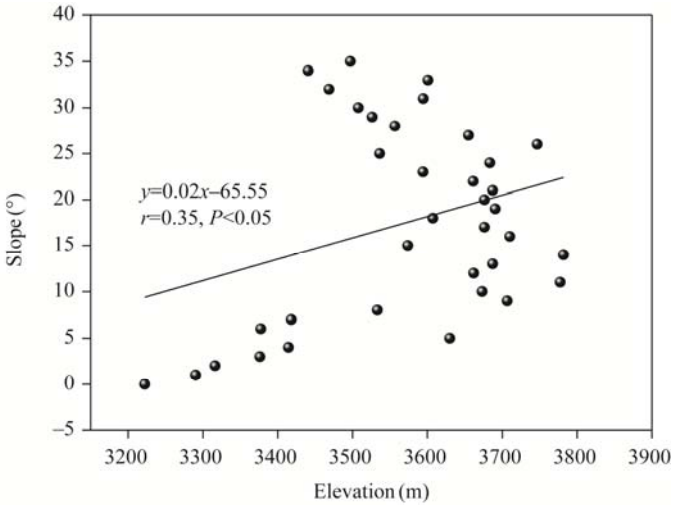

Fig. 11 Relationship between slope and elevation in the QLM

approximately 26.00%–48.00%, while the lowest values (1.00%–4.00%) were recorded in July; the annual mean SCF in these regions ranged from 15.00% to 20.00% (Guo et al., 2022). Compared to the monsoon-dominated basins, the Indus River and Yarkant River (the westerly-dominated regions) exhibited the highest SCF in March and April (46.00%–56.00%); the annual mean SCF in these basins was 33.00%–36.00%, nearly double that observed in monsoon-influenced regions (Guo et al., 2022). This pronounced difference can be attributed to the fact that regions influenced by the westerly circulation could receive up to two-thirds of their annual precipitation in winter and spring (Winiger et al., 2005; Hewitt, 2011). In the QLM, where the influences of monsoons and westerly winds were intertwined, the highest SCF was observed in January, while the lowest occurred in August. The mean annual SCF was 11.49%. The monthly SCF was analogous to that observed in monsoon-dominated regions. Previous studies have reported a decreasing trend in SCF across the QLM and the Qinghai-Xizang Plateau, whereas an increasing trend has been observed in the Altay Mountains and Tianshan Mountains, particularly at higher elevations (Tang et al., 2017; Qin et al., 2022). In this study, the monthly distribution of SCF exhibited a bimodal pattern, aligning with the pattern observed on the Qinghai-Xizang Plateau (Li et al., 2018). Concerning the monthly variation of SCF across different elevation zones, the SCF on the Qinghai-Xizang Plateau reached the highest level in October and April at elevations above 6000 m and remained at the second-highest level in the strong ablation period (July and August); moreover, the lowest SCF occurred in winter (December to February of the following year). In the QLM, we concluded that the SCF similarly reached its highest point in April and November at elevations above 5000 m. However, the lowest SCF occurred in the strong ablation period. These seasonal dynamics are primarily driven by the variation in precipitation form (snowfall and rainfall). Whether it was on the Qinghai-Xizang Plateau or in the QLM, SCF was greater at higher elevations than at lower elevations, and the onset of snowmelt was progressively delayed at higher elevations (Li et al., 2018). Regarding the interannual variation of SCF across different elevation zones, a similar pattern of slight decline was found on the Qinghai-Xizang Plateau and its constituent sub-basins (Yarkant, Indus, Brahmaputra, Salween, etc.) (Guo et al., 2022). Additionally, a slight increasing trend of SCF was observed at elevations below 4000 m, while the opposite trend was evident at higher elevations. In the QLM, a decreasing trend was observed at almost all elevation zones, especially in high-elevation regions. Overall, the reduction rate of SCF increased with the increase of elevations on the Qinghai-Xizang Plateau (Li et al., 2018) and in the QLM (Fig. 5). The reduction in snow cover at high elevations has led to an overall decline in snow cover across the QLM, particularly in winter. Quantitative analysis of meteorological factors indicated that although the increase in winter

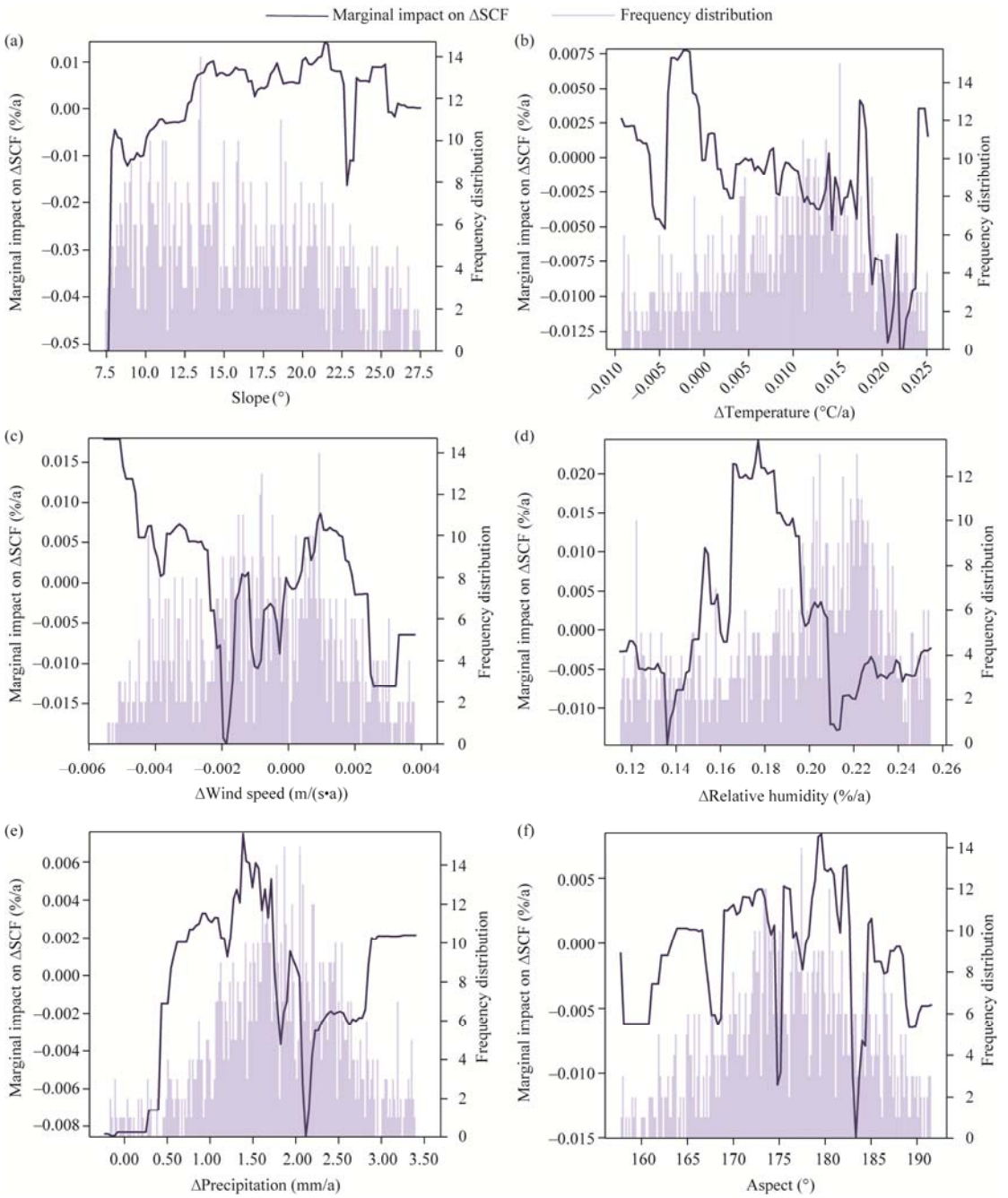

Fig. 12 Partial dependence plots for the impacts of slope (a), temperature (b), wind speed (c), relative humidity (d), precipitation (e), and aspect (f) on SCF change in summer

temperature was relatively minor, the decreases in precipitation and relative humidity were more pronounced in winter than in other seasons. Given that higher relative humidity increases the likelihood of cloud formation and precipitation by bringing the atmosphere closer to saturation, the substantial decline in these variables contributed to the annual reduction in SCF. In spring, SCF was positively correlated with precipitation and negatively correlated with wind speed. A portion of spring precipitation occurred in the form of snowfall, contributing directly to snow accumulation. In contrast, stronger winds markedly enhanced snow sublimation, thereby reducing snow cover, while lower wind speeds favored snow retention. Consequently, the increasing

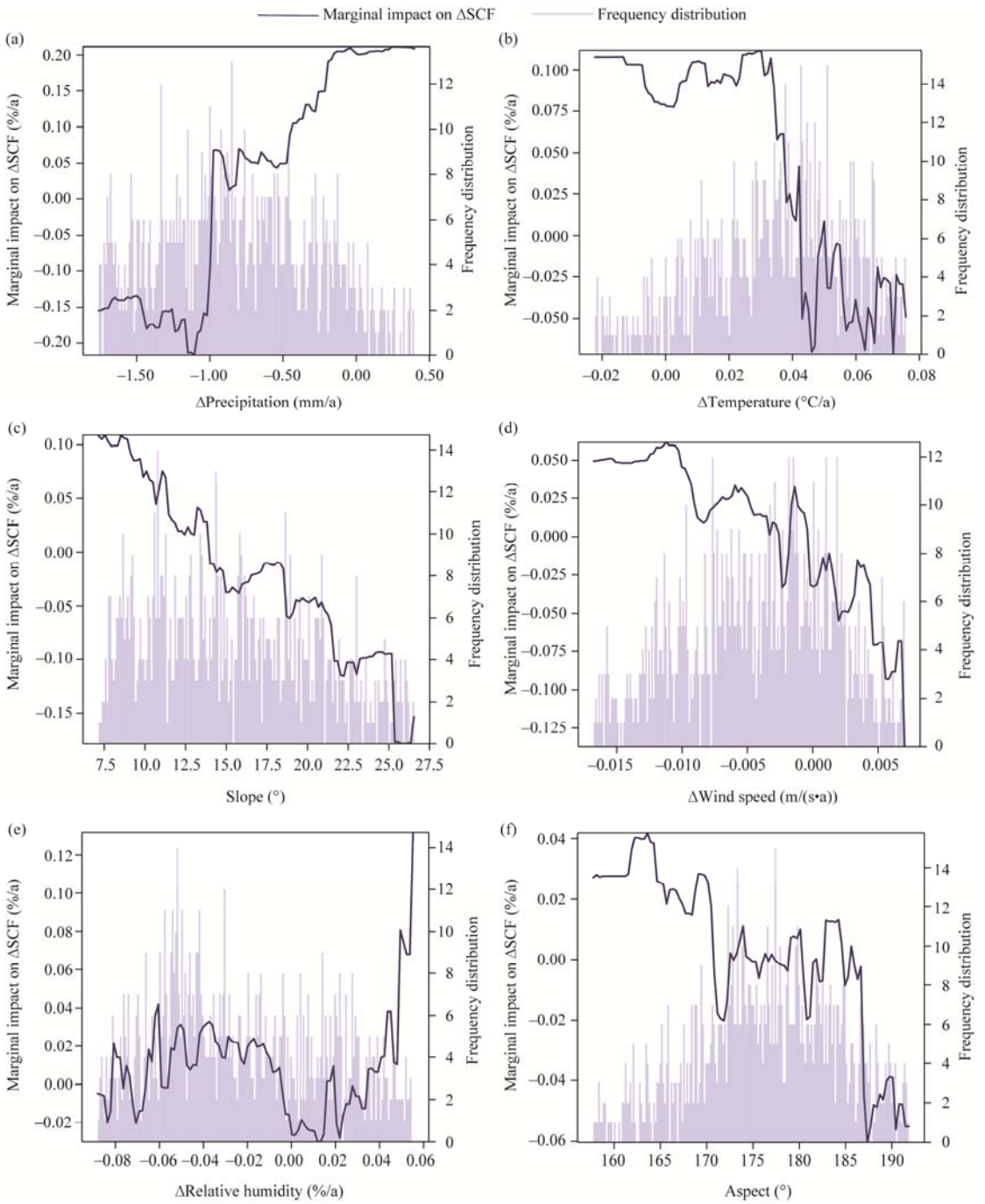

Fig. 13 Partial dependence plots for the impacts of precipitation (a), temperature (b), slope (c), wind speed (d), relative humidity (e), and aspect (f) on SCF change in autumn

precipitation combined with decreasing wind speed led to an overall expansion of spring SCF. In autumn, the declining precipitation coupled with rising temperatures led to a reduction in SCF. Regarding topographical factors, slope greatly influenced SCF change in summer. Despite significant increases in summer precipitation and relative humidity, higher temperatures caused most precipitation to fall as rain rather than snow, enhancing the role of slope. A positive correlation between slope and SCF was observed, primarily because slope increases with elevation, and higher elevations are more conducive to snow accumulation.

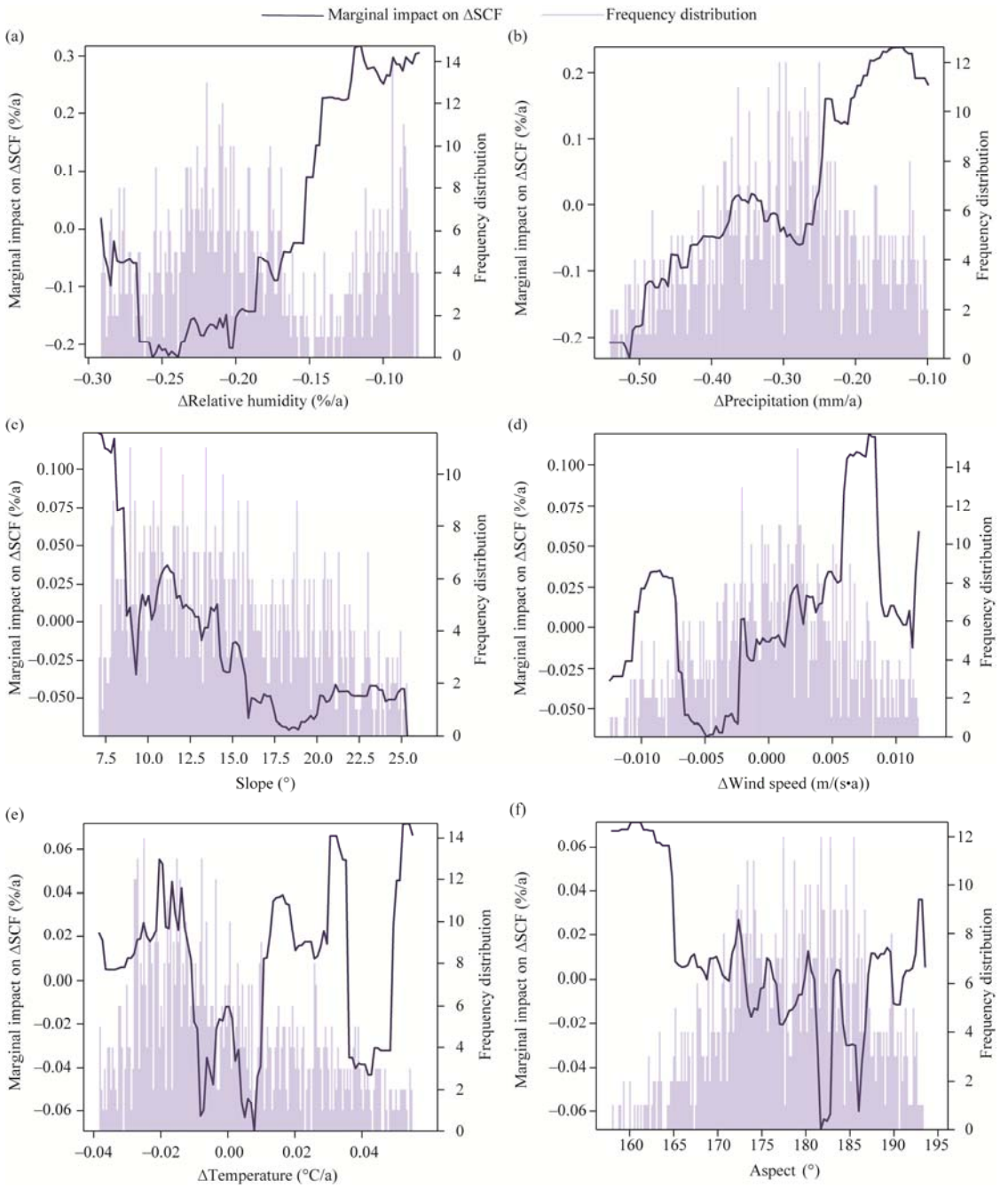

Fig. 14 Partial dependence plots for the impacts of relative humidity (a), precipitation (b), slope (c), wind speed (d), temperature (e), and aspect (f) on SCF change in winter

4.2 Impact of SCF change on surface runoff

The impact of climate change on surface runoff has been extensively studied (Gray et al., 2023; Wang et al., 2023); however, the effect of snow cover in high-altitude mountain areas has been neglected. This study highlighted the significant impact of SCF in winter and spring on surface runoff in spring (Fig. 15). Spring surface runoff indicated a decreasing trend before 2013 but showed an opposite trend after that (coinciding with an increase in spring precipitation after 2013). Overall, spring surface runoff showed a non-significant downward trend during

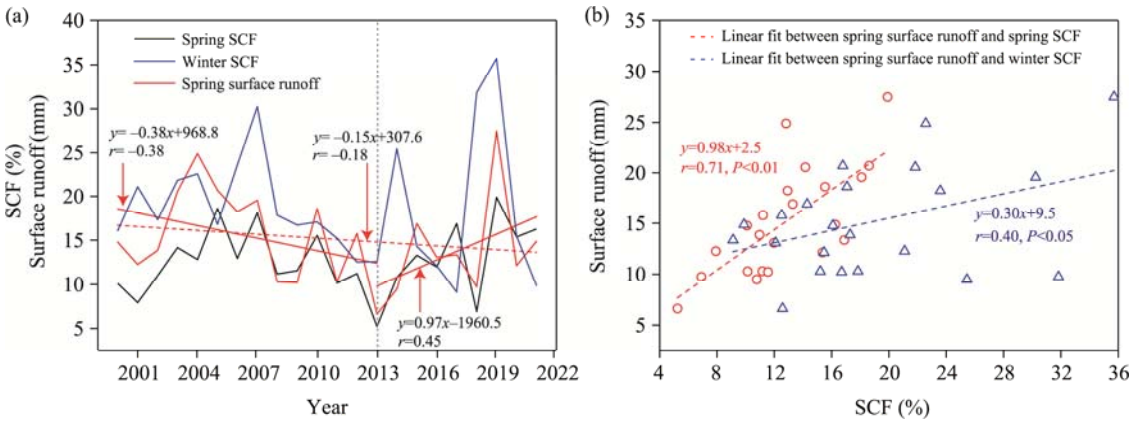

Fig. 15 Variations in spring and winter SCF and spring surface runoff (a) and relationships of spring surface runoff with spring SCF and winter SCF during 2000–2021 (b). The grey dotted line in Figure 15a corresponds to the year when the spring surface runoff undergoes a turning point.

2000–2021, closely aligning with the variation in spring SCF (r=0.71). However, the variation in spring surface runoff was only weakly correlated with winter SCF (r=0.40). These findings indicated that spring SCF exerted a more pronounced influence on spring surface runoff than winter SCF. Furthermore, SCF exerted a stronger influence on runoff than temperature, precipitation, and wind speed in spring and winter, as revealed by PCA. The variance contributions of winter and spring SCF were 42.01% and 46.53%, respectively, considerably higher than those of other meteorological factors, such as winter and spring temperatures, which contributed 27.13% and 24.72%, respectively. The remaining meteorological factors exhibited comparatively smaller variance contributions.

A comparable situation was evident at the spatial scale (Fig. 16). SCF and surface runoff had a strong positive correlation across most of the QLM (P<0.05), especially in the western QLM. This outcome was primarily attributed to the fact that approximately two-thirds of the precipitation in the western QLM dominated by the westerly circulation occurred as snowfall. In contrast, the eastern QLM, which is influenced by the monsoons, has experienced a shift from snowfall to rainfall due to rising temperatures (Hewitt, 2011). The correlation between winter SCF and spring surface runoff was relatively weaker than that between spring SCF and spring surface runoff, particularly in the eastern QLM, where a negative correlation was observed. This outcome can be primarily attributed to the fact that a substantial portion of spring surface runoff in the eastern QLM originates from rainfall rather than snowmelt. Based on PCA, Li et al. (2021) concluded that the influence of temperature on spring runoff was markedly weaker than that of snow cover (there was a high correlation between snow depth during November–March and runoff in April (r=0.84)). A 1.00% change of snow depth during November–March resulted in a 0.43% variation in runoff in April in the source region of the Yellow River, China, which suggested that snow cover has a greater impact on spring runoff. However, substantial uncertainties persist at the annual scale, with precipitation or temperature likely exerting the most pronounced influence (Yan et al., 2023). Understanding the impact of snow cover change on spring runoff is an important scientific foundation for water resource management, ecological conservation, and economic development in the middle and lower reaches of arid areas (Pulliainen et al., 2020). Additionally, the relationship between runoff—especially spring runoff—and precipitation has remained unclear over the past two decades (Ji et al., 2021). Clarifying this relationship is crucial for advancing the present understanding of the underlying drivers of spring runoff variability.

4.3 Uncertainties and limitations

The uncertainties and limitations of this study are mainly reflected in the daily SCF and meteorological datasets. For example, this study found that the trends in SCF for certain elevation

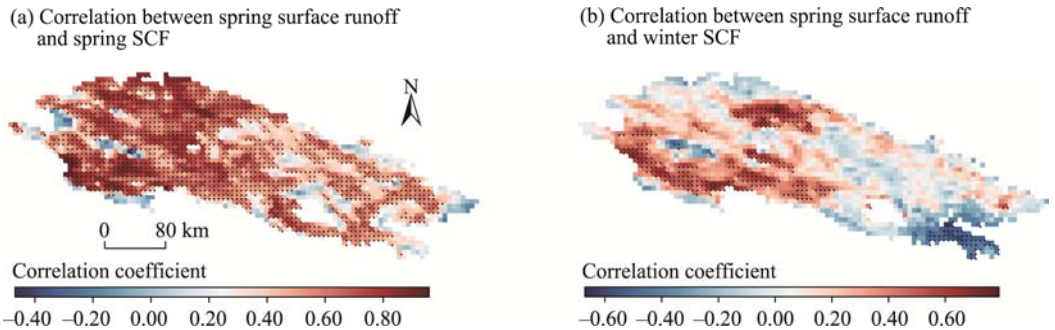

Fig. 16 Correlations of spring surface runoff with spring SCF (a) and winter SCF (b) in the QLM. The black dots indicate the areas showing significant correlation at $P<0.05$ level.

ranges did not pass the significance test ($P>0.05$), potentially due to limitations in the accuracy of remote sensing data and associated retrieval algorithms. The SCF recognition accuracy of the global surface reflectance product MOD09GA/YD09GA was affected by many factors, including cloud cover, terrain, and the relative cloud-free algorithm. Thus, using more advanced retrieval algorithms remains essential to improving SCF estimation accuracy in the QLM. Regarding the meteorological data, this study utilized ERA5-Land reanalysis data with a resolution of 0.1.00°, which could not match the resolution of the SCF data. A straightforward resampling technique, namely bilinear interpolation, was employed for downscaling. Additionally, the accuracy of the ERA5-Land reanalysis data was influenced by the data assimilation methods and forecast models (Wang et al., 2022). These limitations inevitably affect the precision of derived meteorological variables. Future research should integrate additional ground station and remote sensing data, as ground station measurements generally provide higher accuracy than reanalysis data (Hu et al., 2019; Zhang et al., 2019a), while remote sensing products are crucial for capturing the spatial distribution of meteorological variables at finer scales (Wang et al., 2021). Moreover, advanced downscaling techniques such as machine learning are recommended to generate high-resolution meteorological datasets that can better match the resolution of snow cover products.

5 Conclusions

In this study, we analyzed the spatiotemporal variations of SCF in the QLM during 2000–2021, and quantified the impact of meteorological and topographical factors on SCF. The distribution of SCF exhibited considerable spatiotemporal heterogeneity. The SCF was higher in the west and lower in the east. The onset of snowmelt occurred later at higher elevations than at lower elevations. The monthly variation of SCF exhibited a bimodal pattern; the lower the elevation, the closer the occurrence of two peaks. Overall, SCF showed a non-significant decreasing trend from 2000 to 2021. At the annual scale, SCF showed a downward trend in most western regions. However, the opposite trend was observed in some central and eastern regions. Seasonally, SCF exhibited inconspicuous variations in summer. In winter, the east–central region, influenced by the monsoon, showed an upward trend in SCF, whereas the western region, dominated by the westerly circulation, demonstrated a downward trend. Annually, temperature and relative humidity were the most important drivers of SCF change. In spring, precipitation and wind speed were the most influential factors. In summer, slope was identified as the most important factor and the SCF increased with the slope. In autumn, both precipitation and temperature had the greatest impact on SCF. In winter, relative humidity and precipitation were the most important drivers. Concerning the influence of SCF on runoff, the effect of SCF on spring surface runoff was more pronounced in spring than in winter. These findings provide important insights for SCF inversion and simulation, offering valuable guidance for snowmelt water resource management and regional ecological conservation initiatives.

Conflict of interest

The authors declare that they have no known competing financial interests or personal relationships that could have appeared to influence the work reported in this paper.

Acknowledgements

This research was funded by the Key Research and Development Project for Ecological Civilization Construction in Gansu Province (24YFFA010), the Gansu Province Major Science and Technology Project (22ZD6FA005), the Natural Science Foundation of Gansu Province (24JRRA091), the Shanxi Province Basic Research Program (Free Exploration Category) Youth Project (202403021212316), and the Science and Technology Innovation Program for Universities in Shanxi Province (2024L327).

Author contributions

Conceptualization: JIN Zizhen, QIN Xiang; Methodology: JIN Zizhen, LI Xiaoying, ZHANG Jingtian; Formal analysis: ZHAO Qiudong, WANG Chunlin; Writing - original draft preparation: QIN Xiang, MA Xinxin; Writing - review and editing: JIN Zizhen, HE Rui, WANG Renjun; Funding acquisition: JIN Zizhen, QIN Xiang; Supervision: JIN Zizhen, ZHAO Qiudong. All authors approved the manuscript.

References

Barnett T P, Adam J C, Lettenmaier D P. 2005. Potential impacts of a warming climate on water availability in snow-dominated regions. Nature, 438(7066): 303–309.

Chen D L, Xu B Q, Yao T D, et al. 2015. Assessment of past, present and future environmental changes on the Tibetan Plateau. Chinese Science Bulletin, 60(32): 3025–3035. (in Chinese)

Chen X N, Liang S L, Cao Y F, et al. 2016. Distribution, attribution, and radiative forcing of snow cover changes over China from 1982 to 2013. Climatic Change, 137(3): 363–377.

de Jong R, de Bruin S, de Wit A, et al. 2011. Analysis of monotonic greening and browning trends from global NDVI time-series. Remote Sensing of Environment, 115(2): 692–702.

Ding Y J, Qin D H. 2009. Cryosphere change and global warming: Impact and challenges in China. China Basic Science, 11(3): 4–10. (in Chinese)

Elith J, Leathwick J R, Hastie T. 2008. A working guide to boosted regression trees. Journal of Animal Ecology, 77(4): 802–813.

Frei A, Tedesco M, Lee S, et al. 2012. A review of global satellite-derived snow products. Advances in Space Research, 50(8): 1007–1029.

Goodarzi M R, Sabaghzadeh M, Niazkar M. 2023. Evaluation of snowmelt impacts on flood flows based on remote sensing using SRM model. Water, 15(9): 1650, doi: 10.3390/w15091650.

Gray L C, Zhao L, Stillwell A S. 2023. Impacts of climate change on global total and urban runoff. Journal of Hydrology, 620: 129352, doi: 10.1016/j.jhydrol.2023.129352.

Greenacre M, Groenen P J F, Hastie T, et al. 2022. Principal component analysis. Nature Reviews Methods Primers, 3(1): 22, doi: 10.1038/s43586-022-00184-w.

Guo R Y, Ji X, Liu C Y, et al. 2022. Spatiotemporal variation of snow cover and its relationship with temperature and precipitation in the Yarlung Tsangpo-Brahmaputra River Basin. Journal of Mountain Science, 19(7): 1901–1918.

Guo W Q, Liu S Y, Xu J L, et al. 2015. The second Chinese glacier inventory: Data, methods and results. Journal of Glaciology, 61(226): 357–372.

Hewitt K. 2011. Glacier change, concentration, and elevation effects in the Karakoram Himalaya, Upper Indus Basin. Mountain Research and Development, 31(3): 188–200.

Hu G J, Zhao L, Wu X D, et al. 2019. Evaluation of reanalysis air temperature products in permafrost regions on the Qinghai-Tibetan Plateau. Theoretical and Applied Climatology, 138: 1457–1470.

Ji G X, Wu L Y, Wang L D, et al. 2021. Attribution analysis of seasonal runoff in the source region of the yellow river using seasonal Budyko hypothesis. Land, 10(5): 542, doi: 10.3390/land10050542.

Jiang Y Y, Ming J, Ma P L, et al. 2016. Variation in the snow cover on the Qilian Mountains and its causes in the early 21st century. Geomatics, Natural Hazards and Risk, 7(6): 1824–1834.

Jin X, Ke C Q, Xu Y Y, et al. 2015. Spatial and temporal variations of snow cover in the Loess Plateau, China. International Journal of Climatology, 35(8): 1721–1731.

Jolliffe I T, Cadima J. 2016. Principal component analysis: a review and recent developments. Philosophical Transactions of the Royal Society A: Mathematical, Physical and Engineering Sciences, 374(2065): 20150202, doi: 10.1098/rsta.2015.0202.

Kohavi R. 1995. A study of cross-validation and bootstrap for accuracy estimation and model selection. IJCAI'95: Proceedings of the 14th international joint conference on Artificial intelligence–Volume 2. Montreal: Canadian Society for Computational Studies of Intelligence, 1137–1145.

Li C H, Su F G, Yang D Q, et al. 2018. Spatiotemporal variation of snow cover over the Tibetan Plateau based on MODIS snow product, 2001–2014. International Journal of Climatology, 38(2): 708–728.

Li Y, Zhang J F, Zhang J Y, et al. 2015. Research on driving force variation and future trend analysis of ecological evolution of Hexi Corridor. Yellow River, 37(5): 70–73. (in Chinese)

Li Y Z, Qin X, Liu Y S, et al. 2022. Evaluation of long-term and high-resolution gridded precipitation and temperature products in the Qilian Mountains, Qinghai–Tibet Plateau. Frontiers in Environmental Science, 10: 906821, doi: 10.3389/fenvs.2022.906821.

Li Z G, Lyu S H, Chen H, et al. 2021. Changes in climate and snow cover and their synergistic influence on spring runoff in the source region of the Yellow River. Science of the Total Environment, 799: 149503, doi: 10.1016/j.scitotenv.2021.149503.

Li Z X, Yuan R F, Feng Q, et al. 2019. Climate background, relative rate, and runoff effect of multiphase water transformation in Qilian Mountains, the third pole region. Science of the Total Environment, 663: 315–328.

Liang P B, Li Z Q, Zhang H. 2019. Temporal-spatial variation characteristics of snow cover in Qilian Mountains from 2001 to 2017. Arid Land Geography, 42(1): 56–66. (in Chinese)

Lundberg S M, Erion G, Chen H, et al. 2020. From local explanations to global understanding with explainable AI for trees. Nature Machine Intelligence, 2(1): 56–67.

Muñoz-Sabater J, Dutra E, Agustí-Panareda A, et al. 2021. ERA5-Land: A state-of-the-art global reanalysis dataset for land applications. Earth System Science Data, 13(9): 4349–4383.

Notarnicola C. 2020. Hotspots of snow cover changes in global mountain regions over 2000–2018. Remote Sensing of Environment, 243: 111781, doi: 10.1016/j.rse.2020.111781.

Pan F B, Jiang L M, Wang G X, et al. 2024. MODIS daily cloud-gap-filled fractional snow cover dataset of the Asian Water Tower region (2000–2022). Earth System Science Data, 16(5): 2501–2523.

Pedregosa F, Varoquaux G, Gramfort A, et al. 2011. Scikit-learn: Machine learning in Python. The Journal of Machine Learning Research, 12: 2825–2830.

Peng C Y, Sheng Y, Wu J C, et al. 2021. Simulation of the permafrost distribution in the Qilian Mountains. Journal of Glaciology and Geocryology, 43(1): 158–169. (in Chinese)

Pomeroy J W, Stewart R E, Whitfield P H. 2016. The 2013 flood event in the South Saskatchewan and Elk River basins: Causes, assessment and damages. Canadian Water Resources Journal, 41(1–2): 105–117.

Pulliainen J, Luojus K, Derksen C, et al. 2020. Patterns and trends of Northern Hemisphere snow mass from 1980 to 2018. Nature, 581(7808): 294–298.

Qin D H, Liu S Y, Li P J. 2006. Snow cover distribution, variability, and response to climate change in western China. Journal of Climate, 19(9): 1820–1833.

Qin S, Xiao P F, Zhang X L. 2022. How do snow cover fraction change and respond to climate in Altai Mountains of China? International Journal of Climatology, 42(14): 7213–7227.

Ren Z J, Wang J L, Xu H N, et al. 2024. Evolution and driving factors of megadrought and pluvial events in the Qilian Mountains during the past 500 years. Arid Land Geography, 47(2): 214–227. (in Chinese)

Smith T, Bookhagen B. 2018. Changes in seasonal snow water equivalent distribution in High Mountain Asia (1987 to 2009). Science Advances, 4(1): e1701550, doi: 10.1126/sciadv.1701550.

Su F, Zhang L, Ou T, et al. 2016. Hydrological response to future climate changes for the major upstream river basins in the Tibetan Plateau. Global and Planetary Change, 136: 82–95.

Tahir A A, Chevallier P, Arnaud Y, et al. 2015. Snow cover trend and hydrological characteristics of the Astore River basin (Western Himalayas) and its comparison to the Hunza basin (Karakoram region). Science of the Total Environment, 505: 748–761.

Tang Z G, Wang X R, Wang J, et al. 2017. Spatiotemporal variation of snow cover in Tianshan Mountains, Central Asia, based on cloud-free MODIS fractional snow cover product, 2001–2015. Remote Sensing, 9(10): 1045, doi: 10.3390/rs9101045.

Tuttle S E, Cho E, Restrepo P J, et al. 2017. Remote sensing of drivers of spring snowmelt flooding in the north central US. In: Lakshmi V. Remote Sensing of Hydrological Extremes. Springer Remote Sensing/Photogrammetry. Cham: Springer, 21–45.

Wang C L, Si J H, Zhao C Y, et al. 2022. Adequacy of satellite derived data for streamflow simulation in three Hexi inland river basins, Northwest China. Atmospheric Research, 274: 106203, doi: 10.1016/j.atmosres.2022.106203.

Wang J X, Petersen W A, Wolff D B. 2021. Validation of satellite-based precipitation products from TRMM to GPM. Remote Sensing, 13(9): 1745, doi: 10.3390/rs13091745.

Wang Y F, Ye A Z, Zhang Y H, et al. 2023. The quantitative attribution of climate change to runoff increase over the Qinghai-Tibetan Plateau. Science of the Total Environment, 897: 165326, doi: 10.5194/egusphere-egu24-3551.

Wang Y T, He Y, Hou S G. 2007. Analysis of the temporal and spatial variations of snow cover over the Tibetan plateau based on MODIS. Journal of Glaciology and Geocryology, 29(6): 855–861. (in Chinese)

Winiger M, Gumpert M, Yamout H. 2005. Karakorum–Hindukush–western Himalaya: Assessing high-altitude water resources. Hydrological Processes, 19(12): 2329–2338.

Xu J Y, Tang Y, Xu J H, et al. 2022. Impact of snow cover phenology on the vegetation green-up date on the Tibetan Plateau. Remote Sensing, 14(16): 3909, doi: 10.3390/rs14163909.

Xue J, Li Z X, Feng Q, et al. 2023. Ecological conservation pattern based on ecosystem services in the Qilian Mountains, northwest China. Environmental Development, 46: 100834, doi: 10.1016/j.envdev.2023.100834.

Yan W, Wang Y F, Ma X F, et al. 2023. Snow cover and climate change and their coupling effects on runoff in the Keriya River Basin during 2001–2020. Remote Sensing, 15(13): 3435, doi: 10.3390/rs15133435.

Zhang L, Zhang Q, Feng J Y, et al. 2014. A study of atmospheric water cycle over the Qilian Mountains (I): Variation of annual water vapor transport. Journal of Glaciology and Geocryology, 36(5): 1079–1091. (in Chinese)

Zhang L L, Su F G, Yang D Q, et al. 2013. Discharge regime and simulation for the upstream of major rivers over Tibetan Plateau. Journal of Geophysical Research: Atmospheres, 118(15): 8500–8518.

Zhang X Z, Xiong Z, Yan X D. 2019a. Modeling precipitation changes in the Heihe River Basin, Northwest China, from 1980 to 2014 with the Regional Integrated Environment Modeling System (RIEMS) nested with ERA-Interim reanalysis data. Theoretical and Applied Climatology, 137: 493–503.

Zhang Y L, Kang S C, Gao T G, et al. 2019b. Dissolved organic carbon in snow cover of the Chinese Altai Mountains, Central Asia: Concentrations, sources and light-absorption properties. Science of the Total Environment, 647: 1385–1397.

Zhao P, He Z B. 2022. A first evaluation of ERA5-Land reanalysis temperature product over the Chinese Qilian Mountains. Frontiers in Earth Science, 10: 907730, doi: 10.3389/feart.2022.907730.